Agricultural and Forest Meteorology 149 (2009) 1843–1853

Contents lists available at ScienceDirect

Agricultural and Forest Meteorology

journal homepage: www.elsevier.com/locate/agrformet

A comparison of operational remote sensing-based models for estimating crop evapotranspiration

M.P. Gonzalez-Dugo [a,*], C.M.U. Neale [b], L. Mateos [c], W.P. Kustas [d], J.H. Prueger [e], M.C. Anderson [d], F. Li [f]

[a] IFAPA, Centro Alameda del Obispo, Avd. Menéndez Pidal s/n 14080 Córdoba, Spain
[b] Biological and Irrigation Engineering Dept., Utah State University, Logan, UT, USA
[c] Instituto de Agricultura Sostenible, CSIC, Apdo 4084, 14080 Córdoba, Spain
[d] USDA-ARS Hydrology and Remote Sensing Lab, BARC-West, Beltsville, MD, USA
[e] USDA-ARS National Soil Tilth Lab, Ames, IO, USA
[f] Australian Centre for Remote Sensing, Canberra, Australia

ARTICLE INFO

Article history:
Received 31 October 2008
Received in revised form 11 June 2009
Accepted 15 June 2009

Keywords:
Crop evapotranspiration
One-source modeling
Two-source modeling
Crop coefficient
Vegetation index

ABSTRACT

The integration of remotely sensed data into models of evapotranspiration (ET) facilitates the estimation of water consumption across agricultural regions. To estimate regional ET, two basic types of remote sensing approaches have been successfully applied. The first approach computes a surface energy balance using the radiometric surface temperature for estimating the sensible heat flux (H), and obtaining ET as a residual of the energy balance. This paper compares the performance of three different surface energy balance algorithms: an empirical one-source energy balance model; a one-source model calibrated using inverse modeling of ET extremes (namely ET = 0 and ET at potential) which are assumed to exist within the satellite scene; and a two-source (soil + vegetation) energy balance model. The second approach uses vegetation indices derived from canopy reflectance data to estimate basal crop coefficients that can be used to convert reference ET to actual crop ET. This approach requires local meteorological and soil data to maintain a water balance in the root zone of the crop. Output from these models was compared to sensible and latent heat fluxes measured during the soil moisture–atmosphere coupling experiment (SMACEX) conducted over rain-fed corn and soybean crops in central Iowa. The root mean square differences (RMSD) of the estimation of instantaneous latent and heat fluxes were less than 50 W m^{-2} for the three energy balance models. The two-source energy balance model gave the lowest RMSD (30 W m^{-2}) and highest r^2 values in comparison with measured fluxes. In addition, three schemes were applied for upscaling instantaneous flux estimates from the energy balance models (at the time of satellite overpass) to daily integrated ET, including conservation of evaporative fraction and fraction of reference ET. For all energy balance models, an adjusted evaporative fraction approach produced the lowest RMSDs in daily ET of 0.4–0.6 mm d^{-1}. The reflectance-based crop coefficient model yielded RMSD values of 0.4 mm d^{-1}, but tended to significantly overestimate ET from corn during a prolonged drydown period. Crop stress can be directly detected using radiometric surface temperature, but ET modeling approaches-based solely on vegetation indices will not be sensitive to stress until there is actual reduction in biomass or changes in canopy geometry.

1. Introduction

The integration of remotely sensed data into models of evapotranspiration (ET) has broadened the field of application of these models from point to basin and regional scales. Operational applications of remote sensing-based ET models to hydrology and agriculture have increased in the last few years (Allen et al., 2007a). A number of theoretical and experimental studies, addressing both the processing of remote data (Moran et al., 1991; Berk et al., 1998) and flux exchange modeling with limited information (Jackson et al., 1987; Kustas and Norman, 1996), have been necessary to reach the requirements of accuracy and robustness for operational applications.

From these studies, several methods have been developed for estimating ET using remote sensing (see recent review by Kalma

* Corresponding author at: Dpto. de Recursos Naturales y Producción Ecológica, Centro Alameda del Obispo, Instituto de Investigación y Formación Agraria (IFAPA), Alameda del Obispo, s/n, 14004 Córdoba, Spain. Tel.: +34 957 016 030; fax: +34 957 016 043.
E-mail address: mariap.gonzalez.d@juntadeandalucia.es (M.P. Gonzalez-Dugo).

0168-1923/$ – see front matter © 2009 Elsevier B.V. All rights reserved.
doi:10.1016/j.agrformet.2009.06.012

et al., 2008). Two general types of remote sensing approaches for estimating crop ET have been successfully applied in agricultural water use studies. The first approach partitions available energy using the radiometric surface temperature (T_R), derived from thermal band imagery, to constrain the sensible heat flux, computing latent heat as a residual to the surface energy balance (e.g., Moran et al., 1994; Kustas and Norman, 1996; Gillies et al., 1997; Bastiaanssen et al., 1998). A second approach relies on the ability of vegetation indices (VI) derived from surface reflectance data to trace the crop growth and estimate the basal crop coefficient (K_{cb}). The latter method generates spatially distributed values of K_{cb} that capture field-specific crop development (Bausch and Neale, 1989) and are used to adjust a reference ET (ET_o) estimated daily from local weather station data.

Successful applications of the surface temperature approach must address the fact that T_R differs from the aerodynamic temperature, T_o, needed to compute sensible heat, particularly for partial vegetation covered surfaces (Kustas, 1990), and several schemes of varying levels of complexity and input requirements have been formulated to deal with this difference. Some employ empirical/semi-empirical methods for adjusting T_R to T_o, tuned to account for spatial variability in the roughness lengths for heat and momentum transport (e.g., Kustas et al., 1989; Lhomme et al., 1994; Chehbouni et al., 1996; Mahrt and Vickers, 2004). When calibrated with field data, empirical relationships have provided accurate results (Chavez et al., 2005); however, such relationships are typically crop or vegetation specific and are not likely to function correctly when applied to different crop types or landscapes.

A class of internally calibrated surface temperature schemes avoids the problem of specifying T_o by instead modeling the vertical near-surface air gradient $T_A - T_o$. These methods are based on selecting pixels in the satellite image representing the extreme heat and moisture exchanging surfaces (i.e., a dry non-transpiring surface where ET = 0 and a wet surface where ET is at potential) and calculating the spatially distributed sensible heat flux assuming a linear relationship between T_R and the near-surface air temperature gradient across the image (Bastiaanssen et al., 1998). This approach also reduces the need for atmospheric correction of T_R, which is a cumbersome and error-prone process.

Other T_R-based approaches model the effects of partial vegetation cover on T_o using two-source model parameterizations (Shuttelworth and Wallace, 1985; Norman et al., 1995), which partition surface fluxes between the soil and canopy components of the scene. This more physically based approach does not require in situ calibration, although most implementations do require accurate radiometric temperature retrievals. A comparison between a two-source model and an internally calibrated model over different landscapes (Timmermans et al., 2007) showed a reasonable agreement with tower measurements; however, there were significant discrepancies in the heat flux maps generated by the two approaches, particularly for bare soil and sparse canopy covered areas.

Polar-orbiting satellites typically image a scene at best once every couple of days, resulting in instantaneous flux estimates at the time of thermal image acquisition. For most practical applications in water management and agriculture, these instantaneous ET values need to be transformed to daily values. Daily scaling is generally performed by assuming the conservation of a scaling factor determined at the time of imaging, such as the evaporative fraction (Crago and Brutsaert, 1996) or the ratio of actual to reference ET (Allen et al., 2003). Bare soil seems to be the most problematic surface for daily upscaling, since both scaling methods perform well for transpiring crops but poorly for surfaces with low evapotranspiration rates (Colaizzi et al., 2006). Alternatively, geostationary satellites provide surface temperature at hourly timesteps, allowing direct computation of daily fluxes; however, the spatial resolution of such imaging systems is typically too coarse to resolve individual agricultural fields.

The temporal upscaling process is avoided by the VI-basal crop coefficient approach, which provides daily values directly. The details of this approach are discussed below. Another advantage of this approach is that satellite imagery in the reflective bands is more readily available than thermal band data, and generally at higher spatial resolution. However, unless coupled to a soil water balance, this method cannot account either for soil evaporation or the reduction of transpiration due to stomatal closure under water stress conditions. In contrast, surface-temperature-based approaches can readily capture stress effects without requiring ancillary precipitation and soil texture information (Anderson et al., 2007b).

This paper compares the performance of a semi-empirical one-source energy balance model, an internally calibrated T_R scaling model, a two-source energy balance model for estimating sensible and latent heat fluxes from soil and canopy elements, and the vegetation index-basal crop coefficient approach for estimating daily ET. The energy balance models tested basically differ in the method used to estimate sensible heat fluxes. Thus we concentrate on examining those fundamental differences by using measured net radiation and soil heat flux values. The comparison is referenced to an extensive micrometeorological dataset collected during the soil moisture–atmosphere coupling experiment (SMACEX/SMEX02; Kustas et al., 2005) conducted over rain-fed corn and soybean crops in central Iowa.

2. Methodology

2.1. Experimental fields and ground-based measurements

Ground flux measurements were collected during SMACEX/SMEX02 from June 20 to July 9 2002 near Ames, Iowa, on 12 fields, 6 grown with corn and 6 with soybean (Kustas et al., 2005; Fig. 1). During the field campaign, the corn and soybean crops were in their vegetative stage of growth, with leaf area index varying in the soybean fields between 0.8 and 3.1, and in the corn fields between 1.6 and 4.9 (Anderson et al., 2004; see also Table 1).

Each of the 12 fields were equipped with eddy covariance systems mounted on micrometeorological flux towers; 10 fields had a single tower while two fields (one in corn and one in soybean) had an additional tower to sample in-field heterogeneity (Fig. 1). The operational towers for the days and time of the day concerning this study correspond to the fields and days described in Table 1. The setup and characteristics of the flux towers and the processing techniques applied to the datasets are described with detail in Prueger et al. (2005). Data loggers recorded 30-min averaged fluxes and 10-min averaged air temperature and humidity data. The energy balance closure was about 85% (Prueger et al., 2005). In order to compare these data with the model output, which is based on the principle of conservation of energy, closure in the measurements was forced using either the Bowen ratio method or the residual-LE closure method. The first method assumes that the Bowen ratio is correctly measured by the eddy covariance systems and H and LE are rescaled to meet the energy balance while preserving this ratio (Twine et al., 2000). The residual-LE closure method assumes that H is correctly measured, thus the energy balance equation is solved for LE. Brotzge and Crawford (2003) found that the determinations of LE using the eddy covariance method adjusted using the Bowen ratio closure method tended to underestimate LE under high evaporative demand, which may support use of the residual LE-method (e.g., Li et al., 2004). For more details about the field measurements see Kustas et al. (2005) and Prueger et al. (2005).

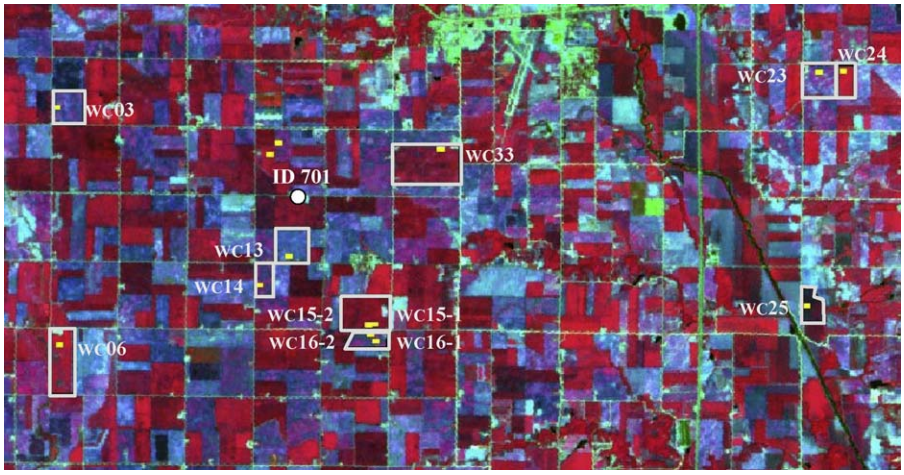

Fig. 1. False color composite of the Landsat ETM-7 image (July 1, 2002; DOY 182) of part of the SMACEX study area at Ames, Iowa, showing the fields that contained the eddy covariance flux stations. The description of the fields is in Table 1 and the yellow polygons represent the upwind averaging areas. ID 701 is the weather station. (For interpretation of the references to color in this figure legend, the reader is referred to the web version of the article.)

Table 1
Average leaf area index, canopy height and ground cover fraction within the flux tower averaging rectangles in each field and on each date selected for the application of the models. Leaf area index and canopy height were estimated from ground cover fraction using experimental equations derived by Anderson et al. (2004).

Field	Crop	Soil type	Leaf area index (m^2/m^2)			Canopy height (m)			Ground cover fraction		
			23 June	1 July	8 July	23 June	1 July	8 July	23 June	1 July	8 July
WC03	Soybean	CANISTEO	0.84	1.63	2.71	0.20	0.31	0.42	0.40	0.64	0.81
WC06	Corn	CLARION	2.53	3.97	4.89	1.08	1.61	1.97	0.82	0.97	0.97
WC13	Soybean	WEBSTER			1.99			0.35			0.72
WC14	Soybean	CLARION	1.45	2.21	3.01	0.29	0.37	0.44	0.63	0.78	0.94
WC15_1	Corn	CANISTEO	2.32	3.58	4.60	1.01	1.46	1.85	0.75	0.88	0.93
WC15_2	Corn	CANISTEO	2.11	3.40	4.48	1.01	1.46	1.85	0.71	0.84	0.92
WC16_1	Soybean	CLARION	1.14	3.08		0.24	0.45		0.53	0.62	
WC16_2	Soybean	CLARION	0.84	1.78		0.20	0.33		0.51	0.70	
WC23	Soybean	CLARION	1.28	1.78		0.26	0.33		0.39	0.69	
WC24	Corn	CLARION		3.74	4.58		1.52	1.85		0.96	0.96
WC25	Corn	SPILLVILLE		2.23	2.53		0.97	1.08		0.60	0.61
WC33	Corn	NICOLLET	1.57	3.16	3.98	0.74	1.31	1.61	0.61	0.87	0.91

2.2. Satellite-based measurements

The remote sensing data used here were acquired by the Landsat 5 and 7 satellites during the experimental period on June 23 (day of year, DOY, 174), July 1 (DOY 182) and July 8 (DOY 189), 2002. The thermal band images were corrected for atmospheric and surface emissivity effects using the atmospheric radiative transfer model MODTRAN 4.1 as described by Li et al. (2004). This correction resulted in at-surface radiometric temperatures. Radiosonde observations collected within the experimental site (fields WC15 and WC16, Fig. 1) during the satellite overpasses, were used along with local sun photometer measurements to obtain the necessary input data for the MODTRAN model. The same model was used to correct the shortwave bands for atmospheric transmittance, obtaining at-surface reflectance values.

Imagery from the Landsat 5 Thematic Mapper (TM) and Landsat 7 Enhanced Thematic Mapper Plus (ETM+) has a nominal pixel resolution of 30 m in the shortwave bands and 60 m (Landsat 7) or 120 m (Landsat 5) in the thermal band.

The prevailing wind direction during all overpasses was from south-southwest. Based on the description of the tower flux footprints in Chavez et al. (2005) (who showed that most footprints were 100–140 m long, with most of the weight concentrated in the first 60 m upwind from the flux stations), model flux estimates were averaged over 120 m × 180 m (4 × 6 shortwave pixels) rectangles centered upwind of each flux tower in the prevalent wind direction.

2.3. Energy balance models for estimating evapotranspiration

2.3.1. One-source models

The latent heat flux (LE, W m^{-2}) can be derived from the energy balance equation as

$$\mathrm{LE} = R_\mathrm{n} - G - H \tag{1}$$

where R_n (W m^{-2}) is net radiation, G (W m^{-2}) soil heat flux and H (W m^{-2}) sensible heat flux. In the application of Eq. (1), R_n and G may be measured values and H can be estimated using the bulk aerodynamic resistance equation:

$$H = \rho C_P \frac{\mathrm{d}T}{r_\mathrm{AH}} \tag{2}$$

where ρ is air density (kg m^{-3}), C_p is the specific heat of air (1005 J kg^{-1} K^{-1}), dT (K) is the temperature gradient between two heights above the surface, z_1 and z_2 (m), and r_AH (s m^{-1}) is the aerodynamic resistance to turbulent transport between z_1 and z_2.

Typically, z_2 is the height above the surface where wind speed and air temperature are measured and z_1 is the height of the zero-plane displacement plus the roughness length. The temperature at this latter height is called aerodynamic temperature (T_o, K). For calculating the aerodynamic temperature over the crops in the SMACEX experiment, Chavez et al. (2005) adjusted an empirical function of the radiometric surface temperature (T_R, K), the air

temperatures (T_A, K), the leaf area index (L), and the wind speed (u, m s^{-1}):

$$T_o = 0.534T_R + 0.39T_A + 0.224L - 0.192u + 1.67 \quad (3)$$

Chavez et al. (2005) computed the aerodynamic resistance, r_{AH}, for stable and unstable atmospheric conditions using the Monin–Obukov similarity theory; the zero-plane displacement height and the roughness lengths for sensible heat and momentum transfer, required for calculating r_{AH}, were obtained after calibrating empirical functions of crop height, using the SMACEX data as well. Since the stability corrections are functions of H, an iterative procedure is needed for computing r_{AH} using this theory. This empirical one-source model was applied as formulated by Chavez et al. (2005), and from here on it will be referred to as 1S-Emp.

The 1S-Emp model has the disadvantage of requiring local calibration using ground-based micrometerological observations. A second single-source model that does not require local calibration, and therefore has more general applicability, was also tested. This approach assumes that the temperature gradient can be approximated by a linear relationship of the surface temperature (Bastiaanssen et al., 1998):

$$dT = a + bT_R \quad (4)$$

where a and b are empirical parameters estimated as described below. Other authors compute an aerodynamic resistance between two near-surface heights above the plant canopy (Allen et al., 2007b) using an iterative stability correction scheme. The wind speed is extrapolated to a "blending height" (200 m) where it is assumed to be uniform and unaffected by surface features. Allen et al. (2007b) contend that by using this approach, the effect of $T_o - T_R$ differences and the variation in the land surface roughness on the relation between dT and T_R in Eq. (4) are minimized.

The parameters a and b are determined by means of a calibration based on the selection of "hot" and "cold" pixels within the satellite scene (Bastiaanssen et al., 1998). The dT values for these two pixels were estimated by rearranging Eq. (2) for the selected "hot" and "cold" pixels and by using Eq. (1) to derive the respective values of H. Following the procedure proposed by Allen et al. (2007b), the "hot" pixel should be bare, dry soil, so LE = 0 and $H = R_n - G$; and the cold pixel should be a well-watered crop at full cover where LE is assumed to be 5% above that of the alfalfa reference evapotranspiration, computed using the standardized ASCE Penman-Monteith equation (ASCE-EWRI, 2005).

This one-source modeling approach for computing H with internalized calibration was applied as formulated by Allen et al. (2007b) in the METRIC model.

2.3.2. Two-source model

The two-source model (2S) used in this study is the updated version of Norman et al.'s (1995) model as presented in Appendix A of Kustas and Norman (1999) and the Appendix of Li et al. (2005). Norman et al.'s model has two variants differing on the assumed resistance network. The variant compared in this study uses the series resistance network. A brief description of the model adapted to our study follows.

The radiometric surface temperature is assumed in the model to be a combination of the soil (T_S) and canopy (T_C) temperatures. When the surface is viewed from nadir, the ensemble radiometric surface temperature is expressed as

$$T_R = \left[f_c T_C^4 + (1 - f_c) T_S^4 \right]^{1/4} \quad (5)$$

where f_c is the fraction of ground covered by the canopy, which is computed as a function of the observed leaf area index.

The energy balance equation can be formulated for the whole canopy-soil system as well as the canopy layer and the soil layer sources as

$$R_n = H + LE + G \quad (6)$$

$$R_{nC} = H_C + LE_C \quad (7)$$

$$R_{nS} = H_S + LE_S + G \quad (8)$$

Each term in Eq. (6) is partitioned between the vegetated canopy and soil, thus:

$$R_n = R_{nC} + R_{nS} \quad (9)$$

$$H = H_C + H_S \quad (10)$$

$$LE = LE_C + LE_S \quad (11)$$

where the subscripts C and S indicate canopy and soil, respectively.

For the series system, where the soil and canopy fluxes interact with each other (Fig. 2), H_C, H_S and H are expressed as

$$H_C = \rho C_p \frac{T_C - T_{AC}}{r_X} \quad (12)$$

$$H_S = \rho C_p \frac{T_S - T_{AC}}{r_S} \quad (13)$$

$$H = H_C + H_S = \rho C_p \frac{T_{AC} - T_A}{r_A} \quad (14)$$

where T_{AC} (K) is the air temperature in canopy-air space, r_X (s m^{-1}) is the total boundary layer resistance of the canopy of leaves, r_S (s m^{-1}) is the resistance to heat flow in the boundary layer immediately above the soil surface, and r_A (s m^{-1}) is the aerodynamic resistance to heat transfer. The expressions for calculating the resistances r_S, r_X, and r_A can be found in Norman et al. (1995); and the expressions for calculating, G, R_{nS} and R_{nC} can be found in Kustas and Norman (1999). LE_C is calculated iteratively using the Priestley–Taylor (PT) approximation (Priestley and Taylor, 1972) as the initial value; and LE_S is calculated as a residual to the overall energy balance. In cases of vegetation stress, the assumed Priestley–Taylor approximation for LE_C results in an unreasonably high T_S which causes a non-physical solution for LE_S, namely <0 or condensation during the daytime. This forces a

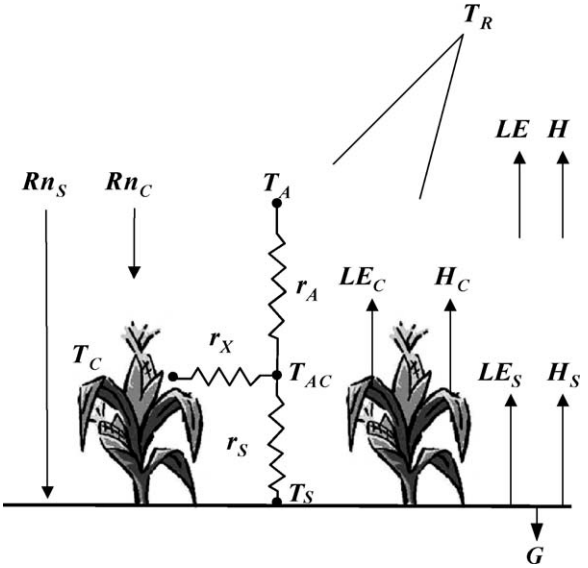

Fig. 2. Schematic illustration of the series resistance network used in the 2S model (Norman et al., 1995). The subscripts C and S indicate canopy and soil, respectively. Symbols are defined in the text.

reduction in the PT parameter (α from its potential ET value of ~1.26) in an iterative process described in Kustas et al. (2004). Eqs. (5)–(14) can be solved for all heat fluxes and the temperatures T_S, T_C and T_{AC} (Norman et al., 1995).

2.3.3. Extrapolation from instantaneous to daily values

Both the one-source and the two-source models provide instantaneous values of heat fluxes corresponding to the time of the satellite overpass (between 10:29 and 10:48 CST, depending on the date and the sensor). However, for most applications an integrated value of the latent heat over the day is more useful. In this paper we explored three methods of extrapolation from instantaneous to daily values.

The first method assumes self-preservation in the diurnal cycle of the energy budget, so that the relative partitioning among the components of the energy balance, expressed by the evaporative fraction [EF = LE/($R_n - G$)], remains constant over the day (Crago, 1996).

Other authors (Gurney and Hsu, 1990; Brutsaert and Sugita, 1992) have pointed out that the EF calculated in morning hours causes an underestimation of daily values, because EF increases slightly into the afternoon. For instantaneous values computed around 5.5 h past sunrise (close to Landsat overpass time), Anderson et al. (1997) found differences of about 10% between estimated and measured daily fluxes. In consequence, these authors suggested the use of an alternative evaporative fraction calculated as

$$\mathrm{EF}' = 1.1\frac{\mathrm{LE}}{R_n + G} \tag{15}$$

The third extrapolation method uses a reference evapotranspiration fraction (Allen et al., 2002a,b, 2007b), assuming that this fraction is relatively constant throughout the day as Romero (2004) demonstrated for several crops, including corn. For consistency with the VI-crop coefficient approach described in the next section, and taking into account a previous comparison conducted by Colaizzi et al. (2006), reference evapotranspiration for grass (ET_o) is used herein instead of the alfalfa reference evapotranspiration used by Allen et al. (2002a,b). Therefore, daily evapotranspiration values (ET_{24}) are computed as

$$\mathrm{ET}_{24} = \left(\frac{\mathrm{ET}}{\mathrm{ET_o}}\right)\mathrm{ET}_{o24} \tag{16}$$

where ET and ET_o are the instantaneous crop and reference evapotranspiration values and ET_{o24} is daily reference evapotranspiration, calculated using the Penman–Monteith equation (Monteith and Unsworth, 1990; Allen et al., 1998). Note that the ratio ET/ET_o in Eq. (16) is equivalent to the crop coefficient for the day of concern (as described in the next section).

2.4. Vegetation index derived crop coefficient

Daily ET was also computed using FAO methodology, based on the concepts of crop coefficient and reference ET (Doorembos and Pruitt, 1977). Reference evapotranspiration (ET_o, mm) was estimated using the Penman–Monteith equation with hourly data of solar radiation, wind speed, air temperature and relative humidity supplied by a weather station centered in the study area (ID 701, Fig. 1). The crop coefficient (K_c) relates the evapotranspiration of a given crop to that of a reference surface, and was derived using the dual approach (Wright, 1982) in the form popularized in the FAO56 manual (Allen et al., 1998). This approach separates crop transpiration (represented by the basal crop coefficient, K_{cb}) from soil surface evaporation as follows:

$$\mathrm{ET} = (K_{cb}K_s + K_e)\mathrm{ET}_o \tag{17}$$

where K_s quantifies the reduction in crop transpiration due to soil water deficit and K_e is the soil evaporation coefficient, obtained by calculating the amount of energy available at the soil surface as

$$K_e = K_r(K_{c\,max} - K_{cb}) \tag{18}$$

where K_r is a dimensionless evaporation reduction coefficient dependent on topsoil water depletion (Allen et al., 1998) and $K_{c\,max}$ is the maximum value of K_c following rainfall or irrigation. The value of K_e cannot be greater than the product $f_{ew} \times K_{max}$, where f_{ew} is the fraction of the soil surface that is both exposed and wetted.

Vegetation indices (VIs) are transformations of two or more spectral bands designed to assess vegetation condition, foliage, cover, phenology, and processes related to the fraction of photosynthetically active radiation absorbed by a canopy (fPAR) (Glenn et al., 2008). The fact that both the basal crop coefficient, K_{cb}, and VIs are sensitive to leaf area index (L) and ground cover fraction (f_c) (Neale et al., 1989; Choudhury et al., 1994) supports the estimation of crop coefficients from spectral measurements. Based on this assumption and the fact that K_{cb} peaks before full ground cover, Gonzalez-Dugo and Mateos (2008) derived a linear equation to compute K_{cb} from SAVI (the soil adjusted vegetation index, Huete, 1988). A modification of this equation (that avoids the adjustment function of the crop height) has been used here:

$$K_{cb} = \frac{K_{cb,mx}}{f_{c,mx}}\left(\frac{\mathrm{SAVI} - \mathrm{SAVI_{min}}}{\mathrm{SAVI_{max}} - \mathrm{SAVI_{min}}}\right) \quad \text{if} \quad f_c < f_{c,mx} \tag{19a}$$

$$K_{cb} = K_{cb,max} \quad \text{if} \quad f_c \geq f_{c,mx} \tag{19b}$$

where the subscripts max and min refer to the values of SAVI for very large L and bare soil, respectively, and $f_{c,mx}$ is the f_c at which K_{cb} is maximal ($K_{cb,mx}$) (Table 2).

In order to compute K_e and K_s in Eq. (17), it was essential to carry out a soil root zone water balance and to obtain information regarding the occurrence of soil wetting by rainfall. The root zone depth (Z_r) was computed as a function of K_{cb}:

$$Z_r = Z_{r\,min} + (Z_{r\,max} - Z_{r\,min})\frac{K_{cb}}{K_{cb\,max}} \tag{20}$$

where $Z_{r\,max}$ and $Z_{r\,min}$ are the maximum effective root depth and the effective root depth during the initial stage of crop growth (Table 2). The change in the root zone water content, ΔS_w, is computed as the difference between the water inflows and outflows:

$$\Delta S_w = S_{Wf} - S_{Wi} = R - \mathrm{ET} - D \tag{21}$$

where S_{Wf} and S_{Wi} (mm) are the root zone water content at the beginning and end of the water balance period, R is infiltrated rainfall and D is deep drainage, both during the water balance period. Eq. (21) may be expressed in terms of root zone water

Table 2
Crop parameters used for deriving the crop coefficients and computing the water balance following the procedure described in FAO Irrigation and Drainage Paper No. 56 (Allen et al., 1998).

Parameter	Soybean	Corn
Maximum crop height	0.6 m	2.0 m
Maximum effective root depth ($Z_{r\,max}$)	1.1 m	1.2 m
Minimum effective root depth ($Z_{r\,min}$)	0.1 m	0.1 m
$SAVI_{max}$	0.75	0.75
$SAVI_{min}$	0.1	0.1
Maximum basal crop coefficient ($K_{cb,max}$)[a]	1.06	1.09
Ground cover fraction for $K_{cb,max}$ ($f_{c,mx}$)	0.80	0.80

[a] Typical values adjusted for local relative humidity and wind speed.

Table 3
Soils parameters used for computing the water balance following the procedure described in Allen et al. (1998), being θ_{FC} the soil water content at field capacity, θ_{WP} the soil water content at wilting point, Z_e the depth of soil surface evaporation layer, TEW the total evaporable water and REW the readily evaporable water.

Parameter	Soil type				
	Canisteo	Webster	Nicollet	Clarion	Spillville
Texture class	Silt Clay Loam	Silt Clay Loam	Loam	Loam	Loam
θ_{FC} ($m^3\ m^{-3}$)	0.30	0.30	0.30	0.31	0.31
θ_{WP} ($m^3\ m^{-3}$)	0.12	0.12	0.12	0.15	0.15
Z_e (m)	0.1	0.1	0.1	0.1	0.1
TEW (mm)	24	24	24	23.5	23.5
REW (mm)	10	10	10	10	10

deficit computed daily:

$$\mathrm{RZWD}_i = \mathrm{RZWD}_{i-1} + \mathrm{ET}_i + D_i - R_i \quad (22)$$

where the subscript i indicates the day of concern and RZWD_i and RZWD_{i-1} are the root zone water deficits on days i and $i-1$, respectively.

It is understood that the root zone is full of water, RZWD = 0, when its water content is at field capacity, and that it is empty when the water content is at the wilting point. The root zone water holding capacity (RZWHC) is the depth of water between these two extremes.

The stress coefficient, K_s, is computed based on the relative root zone water deficit as:

$$K_s = \frac{\mathrm{RZWHC} - \mathrm{RZWD}_i}{(1-p)\mathrm{RZWHC}} \quad \text{if } \mathrm{RZWD}_i < (1-p)\mathrm{RZWHC} \quad (23a)$$

$$K_s = 1 \quad \text{if } \mathrm{RZWD}_i \geq (1-p)\mathrm{RZWHC} \quad (23b)$$

where p is the fraction of the RZWHC below which transpiration is reduced.

The water balance computation was initiated in November 2001 and simulated under different starting soil moisture conditions, with all cases indicating that on May 1, 2002, the root zone could be assumed to be at field capacity due to several important rainfall events that occurred at the end of April. Daily rainfall data were obtained from the rain gauge network of the National Soil Tilth Research Laboratory, selecting the rain gauge nearest to each averaging rectangle. The soil parameters necessary for applying the soil water balance were obtained by identifying the dominant soil class (Miller, 2006) in each averaging rectangle, consulting the description of the typical soil profile (Soil Survey Staff, NRCS, 2008) of the pertinent soil classes and selecting from Table 19 in Allen et al. (1998) the appropriate values of soil water content at field capacity and wilting point for each averaging rectangle (Table 3).

3. Results

3.1. Comparison of instantaneous fluxes

The comparison between the H and LE predictions from the three energy balance models with measured values is depicted in Fig. 3, with statistics presented in Table 4. The measured LE data in Fig. 3 were obtained by forcing closure using the residual method. An overall good agreement between the estimated and measured fluxes was found for all models. The root mean square differences (RMSD) and absolute mean bias errors (MBE) in model estimates of both LE and H were less than or equal to 50 W m^{-2} and 33 W m^{-2}, respectively, for the three models (Table 4). The ranking in performance as measured through the RMSD was 2S, METRIC, 1S-Emp; and the ranking as measured through the MBE was METRIC, 2S, 1S-Emp. The 2S model provided the best overall r^2 values.

In order to evaluate model performance for operational applications, the values of T_A and u used in Eq. (3) in the computation of the aerodynamic resistances and in the computation of the sensible heat fluxes were taken from a standard meteorological station located in the study area (ID 701, Fig. 1), rather than from the flux towers themselves. When the models were run with the input values of T_A and u measured at the flux towers, the agreement between predicted and observed data was marginally improved for the 2S model, and significantly improved for the 1S-Emp model, but did not appreciably affect the performance of METRIC. This difference among models was due to the fact that the METRIC model does not use T_A, except for estimating the cold pixel LE reference value and it uses u only for computing wind speed at the 200 m blending height, while the 2S and 1S-Emp models use T_A for calculating sensible heat fluxes and use u for the calculation of the aerodynamic resistances. In addition, the 1S-Emp model calculates the aerodynamic temperature as a function of T_A and u with Eq. (3) calibrated using values measured at the flux towers. In the case of the 1S-Emp model, using the flux tower T_A and u, instead of the values obtained at the weather station, reduced the RMSE of the LE predictions from 50 to 38 W m^{-2} and the MBE from 33 to 12 W m^{-2}, and increased the r^2 from 0.83 to 0.91.

The predictions of the 2S model were consistent with previous calculations by Li et al. (2005) using data from the same field campaign, and improved slightly the results obtained with the parallel resistance formulation presented by Gonzalez-Dugo et al. (2006).

On the other hand, the flux tower sites did not sample fields with bare soil, the type of surface where Timmermans et al. (2007) found greater discrepancies between the 2S model (which showed good agreement with the observations) and SEBAL (Bastiaanssen et al., 1998), the model that pioneered the use of a linear relationship between T_R and dT (Eq. (4)) for computing H. Moreover, the variation in surface roughness or vegetation water stress across the scenes was relatively small in our study (Norman et al., 2006), a condition under which a unique linear relationship between dT and T_R is more likely to exist.

A major disadvantage of the 2S and 1S-Emp models is the need for atmospheric and emissivity correction of the thermal infrared imagery to obtain land surface temperature. For the uncertainty of ±1.5 °C and ±1 °C for Landsat-5 and Landsat-7, respectively, in the determination of T_R reported by Li et al. (2004), the variation of H in our experimental conditions would be in the range of 20–25 W m^{-2} for the 2S and 35–40 W m^{-2} for the 1S-Emp model, on average. These variation produce an increase of the RMSD of H estimations compared to measured values of 11 W m^{-2} on average for the TSM and by 18 W m^{-2} for the 1S-Emp the RMSD. However, techniques using time-differencing in surface temperature developed by Anderson et al. (1997) and Norman et al. (2000) built on the 2S algorithm, have shown to be much less sensitive to errors in T_R. The atmosphere land exchange inverse (ALEXI) scheme, which is coupled to an atmospheric boundary layer model, does not require air temperature observations or highly accurate atmospherically emissivity corrected T_R observations (Anderson et al., 2007a).

Similarly, the scene internal calibration of the METRIC model greatly reduces the need for an accurate atmospherically and emissivity corrected land surface temperature. However, the selection of the cold and hot pixels that are needed instead entails some degree of subjectivity. For this reason, we explored the effect of different selected extreme temperature pixel values on the estimation of H. Three different observers trained in the processing of satellite images were asked to select the cold and hot pixels in the three Landsat images. The three observers had to follow a

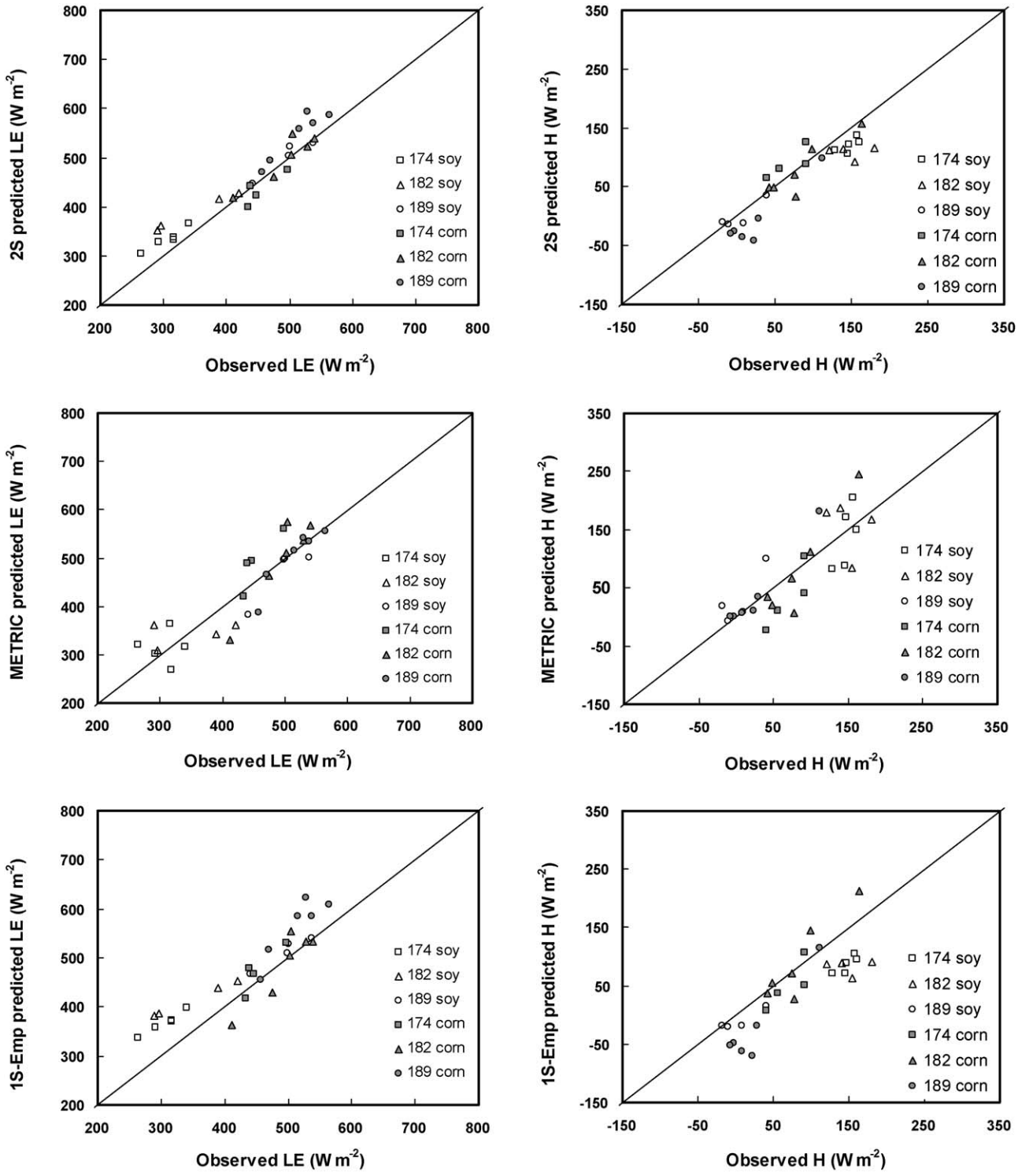

Fig. 3. Comparison of the instantaneous sensible heat (H) and latent heat (LE) estimates using the 2S, METRIC and 1S-Emp models and measured H, and the residual closure adjusted LE values measured by the flux tower network. The symbols correspond to the crop type and the date of measurement for each field.

Table 4
Statistical performance of the two-source (2S), one-source empirical (1S-Emp), and one-source internalized calibration (METRIC) models for estimating instantaneous sensible (H) and latent (LE) heat fluxes. N is the number of observations; RMSD is the root mean square difference; MBS the mean bias error, and r^2 the correlation coefficient.

Flux	N	RMSD (W m^{-2})			MBE (W m^{-2})			r^2		
		2S	1S-Emp	METRIC	2S	1S-Emp	METRIC	2S	1S-Emp	METRIC
H	29	30	50	42	17	−33	−1	0.83	0.70	0.70
LE	29	30	50	42	17	33	1	0.92	0.83	0.81

Table 5
Statistical performance for instantaneous and daily results of the METRIC model with three sets of extreme pixel values selected by different operators. The subscripts BR and RA refer to Bowen ratio and residual adjustment methods to force closure, respectively.

Operator	Instantaneous values								Daily values of ET		
	N[a]	RMSD[b] (W m^{-2})			r^2				N[a]	RMSD[b] (mm d^{-1})	r^2
		H	H_{BR}	LE_{BR}	H	LE_{RA}	H_{BR}	LE_{BR}			
A	29	42	44	40	0.70	0.81	0.73	0.86	27	0.58	0.76
B	29	47	39	35	0.76	0.83	0.79	0.89	27	0.78	0.80
C	29	53	48	44	0.69	0.81	0.68	0.85	27	0.89	0.74

[a] Number of observations.
[b] Root mean square difference.

Table 6
Statistical performance of the two-source (2S), one-source empirical (1S-Emp), and one-source internalized calibration (METRIC) models for estimating daily evapotranspiration using three methods to scale from instantaneous to daily values: reference evapotranspiration fraction (ET_0F), evaporative fraction (EF) and 1.1 times the evaporative fraction (EF′). And statistical performance of the FAO—vegetation index method for estimating evapotranspiration (FAO-VI).

Scaling method	N[a]	RMSD[b] (mm d^{-1})			MBE[c] (mm d^{-1})			r^2		
		2S	1S-Emp	METRIC	2S	1S-Emp	METRIC	2S	1S-Emp	METRIC
ET0F	27	0.74	0.84	0.76	0.38	0.59	0.07	0.76	0.84	0.76
EF	27	0.64	0.58	0.92	−0.52	−0.32	−0.80	0.81	0.70	0.76
EF′	27	0.39	0.57	0.58	−0.05	0.27	−0.25	0.81	0.70	0.76
FAO-VI	27		0.42			0.01			0.70	

[a] Number of observations.
[b] Root mean square difference.
[c] Mean bias error.

common procedure (Allen et al., 2002a,b). The mean differences found in the selection of extreme values between the operators were of 0.5 °C for the cold pixel and 1 °C for the hot pixel, with maximums of 1.2 and 2.2 °C, respectively, for specific dates. The average difference in H values obtained with the three sets of hot/cold pixel is 25 W m^{-2}. The general results of the model application are presented in Table 5 and indicate that differences in the hot and cold pixel selections did not significantly affect model performance. The results used for models comparison (Tables 4 and 6) correspond to the set of extreme values selected by operator *A*, which yielded the lowest RMSD in daily integrated latent heating.

3.2. Comparison of daily ET

The results of the daily integration of latent heat performed using the three scaling methods discussed in Section 2.3.3 (evaporative fraction, adjusted evaporative fraction and reference ET fraction) are presented in Table 6. The three energy balance models behaved similarly in relation to each method of integration. The adjusted evaporative fraction method using a correction factor of 1.1 yielded the best results (lowest RMSD). The negative mean bias error found when using the evaporative fraction method for mid morning measurements (Table 6) confirmed previous findings (Brutsaert and Sugita, 1992). The MBE was reduced using the 1.1 factor introduced in Eq. (15), while flux observations from SMACEX suggest an optimal value of 1.14 (Fig. 4).

Fig. 5 depicts the relationship between daily measured ET and estimates from the three energy balance models extrapolated from instantaneous values using the adjusted EF method, along with ET values estimated with the VI-basal crop coefficient approach. The data points were reasonably close to the 1:1 line, with an RMSD of less than 0.60 mm d^{-1} for all models (Table 6). The 1S-Emp model slightly overestimated daily ET, as was observed for the instantaneous flux comparisons. Although the METRIC model reproduced instantaneous ET well, it underestimated daily ET by 0.25 mm d^{-1}. This bias disappeared when the ET_0F scaling method proposed in Allen et al. (2007b) was used, although RMSD increased (Table 6). The RMSD and MBE for the FAO-VI model were comparable to those of the energy balance models, although the correlation coefficient was smaller (Table 6).

The absence of rain during the period between DOY 172–187 increased the root zone water deficit, causing water stress in some crop patches (Anderson et al., 2004). The effect of this water stress showed up in the ground measurements in the corn fields on DOY 182, but it was not predicted by the FAO-VI model. For this model, 6 out of the 8 corn data points for DOY 182 were above the 1:1 line, overestimating daily ET by 1 mm day^{-1} on average (Fig. 5d). One possible reason for this overestimate could be that the soil water model simulations used in the FAO-VI model were non-representative of the local crop conditions, due either to spatial variability in rainfall or sub-optimal specification of soil hydraulic parameters, resulting in an underprediction of the RZWD and overprediction of K_s.

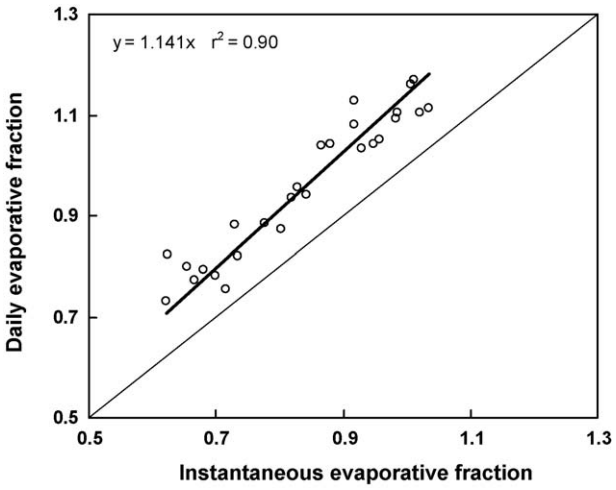

Fig. 4. Instantaneous evaporative fraction (10:30–11 CST) *vs.* daily evaporative fractions computed from the flux tower measurements.

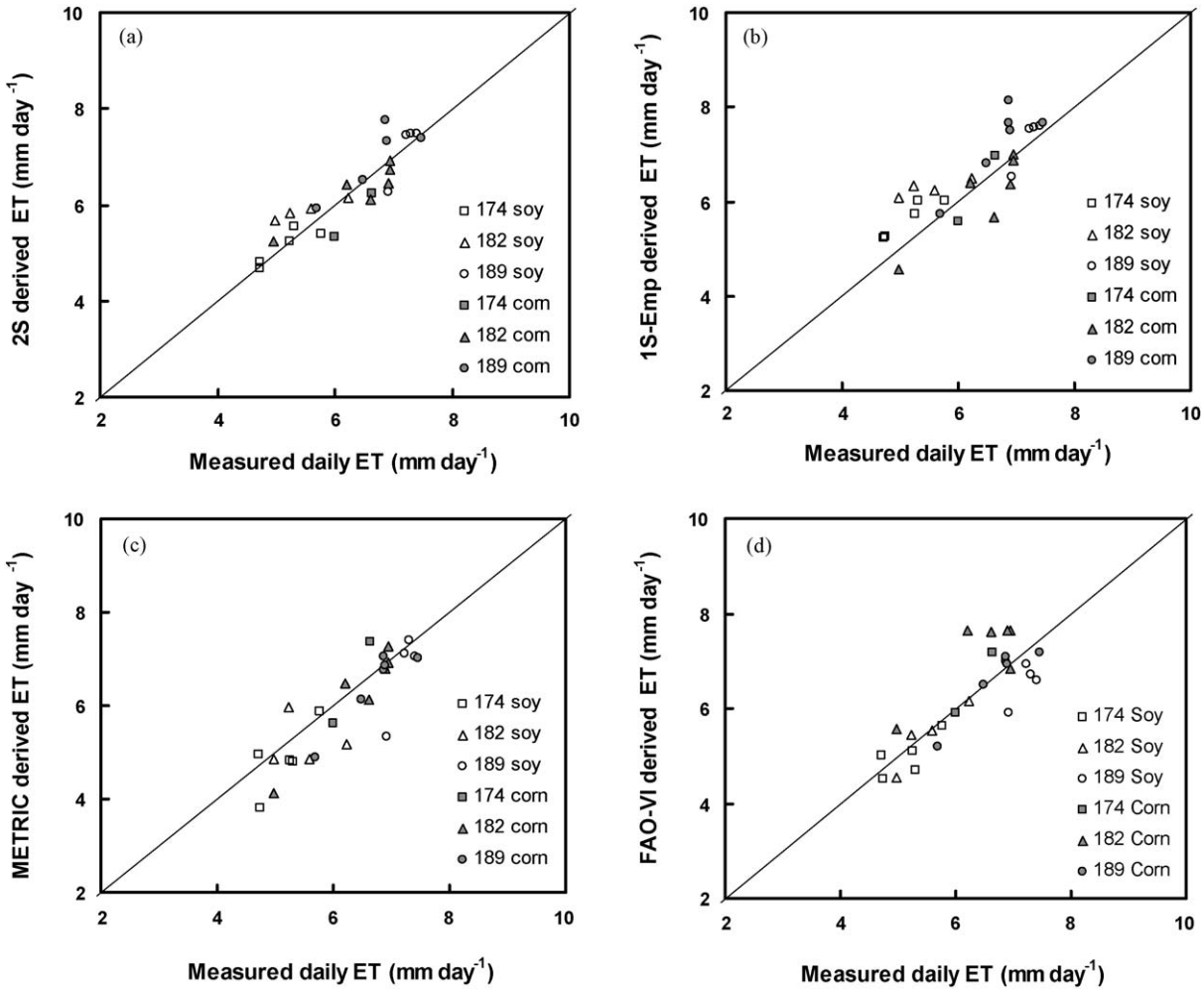

Fig. 5. Daily latent heat estimates produced by the four models compared with the daily values measured by the flux tower network.

4. Discussion and conclusions

Crop evapotranspiration estimates from two types of remote sensing models were compared with flux observations from 10 field sites in a rain-fed corn and soybean production region in central Iowa. The first type (based on the surface energy balance) requires measurements of radiative temperature, with ancillary computations using the red and near-infrared spectral band reflectance. The second type (VI-basal crop coefficient) requires only red and near-infrared spectral band reflectances as remotely sensed inputs.

Three variants of thermal-based energy balance models were compared. Among these, the 2S model has a higher degree of physical realism than the 1S-Emp and the METRIC models, while requiring similar input information. In the estimation of instantaneous heat fluxes, the 2S model marginally outperformed both one-source modeling schemes, although all three models gave satisfactory results. It should be stressed that the results presented herein used measured values of R_n and G for the three energy balance models. Since LE is obtained by residual to the surface energy balance, inter-model discrepancies are likely to be greater when using model estimates of R_n and G.

The 1S-Emp model, with aerodynamic temperature obtained from a locally calibrated empirical function, has limited applicability to environments where calibration of the radiometric–aerodynamic relation is not performed a priori. Performance of the 1S-Emp model degraded significantly when non-local meteorological data were used to drive the model, as would be the case in most operational applications. Previous research has proven the validity of the 2S model in other environments (Kustas and Norman, 1997), while some conceptual issues pointed out by Norman et al. (2006) and model intercomparisons over actual landscapes (Timmermans et al., 2007) raise concern about the application of models with internalized calibration, based on the selection of cold and hot pixels, over heterogeneous scenes.

Thermal satellite images used by 2S or 1S-Emp models require atmospheric correction and calibration to obtain accurate land surface temperatures. However T_R time differencing technique is shown to significantly reduce this dependency. The internal calibration approach using maximum and minimum T_R to constrain energy partitioning for the limits ET∼0 and ET = ET_o in the METRIC approach minimizes the need for atmospheric corrections. However, this approach also assumes both ET extremes exist within the satellite scene, which is not as likely in rain-fed agricultural areas.

An important step in the application of the remote sensing energy balance models is the extrapolation from instantaneous to daily and seasonal values which are of more value for agricultural purposes. For clear days, instantaneous values may be extrapolated to daily values, but the extrapolation factor must be selected carefully. It is likely that the extrapolation to daily values on days with different conditions to the typical clear day will not perform as well.

The FAO-VI model provides daily rather than instantaneous crop evapotranspiration, and therefore does not require additional

processing for daily extrapolation. If this method is to be properly applied, however, reliable rainfall and reference evapotranspiration data must be available over the modeling region at spatial resolutions resolving typical heterogeneity in the soil moisture distribution. Surface networks at this scale are scarce, and therefore in practice this information must be derived through a combination of ground and satellite information and weather prediction models.

Since the thermal-based energy balance models inherently account for ET reduction due to plant water stress, these models are more suitable than the FAO-VI model for estimating crop ET under conditions of moisture stress. In these models, the elevated canopy temperatures detected in the thermal band serve as an effective proxy for precipitation data, providing a remote indicator of depleted root zone available water (Hain et al., in press). These applications underscore the value of maintaining global thermal imaging sensors capable of resolving individual agricultural fields (Anderson and Kustas, 2008).

Acknowledgements

The authors would like to recognize the funding provided by NASA Grant S-44825-G under NRA 00OES-07 from the NASA Terrestrial Hydrology Program, INIA through project RTA2005-047 and contract NAG5-11673 with Utah State University. Additional support was provided though the Cooperative Research Program of the Organization for Economic Cooperation and Development (OCDE). C.M.U. Neale was also supported by a grant from the MEC of Spain, SAB2004-0200.

References

Allen, R.G., Morse, A., Tasumi, M., 2003. Application of SEBAL for western U.S. water rights regulation and planning. In: Proceeding of the ICID International Workshop on Remote Sensing, Montpellier.

Allen, R.G., Morse, A., Tasumi, M., Trezza, R., Bastiaanssen, W.G.M., Wright, J.L., Kramber, W., 2002a. Evapotranspiration from a satellite-based surface energy balance for the Snake River Plan aquifer in Idaho. In: Proceeding of the USCID/EWRI Conference on Energy, Climate, Environment, and Water. U.S. Committee on Irrigation and Drainage, Denver, CO.

Allen, R.G., Tasumi, M., Trezza, R., Waters, R., 2002. METRICtm. Mapping evapotranspiration at high resolution and using internalized calibration. Advanced Training and Users Manual. Version 1.0.

Allen, R.G., Pereira, L.S., Raes, D., Smith, M., 1998. Crop evapotranspiration. Guidelines for computing crop water requirements. FAO Irrigation and Drainage Paper No. 56, Rome, Italy.

Allen, R.G., Tasumi, M., Morse, A., Trezza, R., Wright, J.L., Bastiaanssen, W., Kramber, W., Lorite, I.J., Robison, C.W., 2007a. Satellite-based energy balance for mapping evapotranspiration with internalized calibration (METRIC)—applications. J. Irrig. Drain. Eng. ASCE 133 (4), 395–406.

Allen, R.G., Tasumi, M., Trezza, R., 2007b. Satellite-based energy balance for mapping evapotranspiration with internalized calibration (METRIC)—model. J. Irrig. Drain. Eng. ASCE 133 (4), 380–394.

Anderson, M.C., Neale, C.M.U., Li, F., Norman, J.M., Kustas, W.P., Jayanthi, H., Chavez, J., 2004. Upscaling ground observations of vegetation water content, canopy height, and leaf area index during SMEX02 using aircraft and Landsat imagery. Remote Sens. Environ. 92, 447–464.

Anderson, M.C., Norman, J.M., Diak, G.R., Kustas, W.P., Mecikalski, J.R., 1997. A two-source time-integrated model for estimating surface fluxes using thermal infrared remote sensing. Remote Sens. Environ. 60, 195–216.

Anderson, M.C., Norman, J.M., Kustas, W.P., 2007a. Upscaling flux observations from local to continental scales using thermal remote sensing. Agron. J. 99, 240–254.

Anderson, M.C., Norman, J.M., Mecikalski, J.R., Otkin, J.A., Kustas, W.P., 2007b. A climatological study of evapotranspiration and moisture stress across the continental U.S. based on thermal remote sensing. I. Model formulation. J. Geophys. Res. 112, D10117.

Anderson, M., Kustas, W., 2008. Thermal remote sensing of drought and evapotranspiration. EOS Trans. AGU 89 (26), doi:10.1029/2008EO260001.

ASCE-EWRI, 2005. The ASCE standardized reference evapotranspiration equation. In: ASCE-EWRI Standardization of Reference Evapotranspiration Task Committee Rep., ASCE, Reston, VA.

Bastiaanssen, W.G.M., Menenti, M., Feddes, R.A., Holstlag, A.A.M., 1998. A remote sensing surface energy balance algorithm for land (SEBAL). 1. Formulation. J. Hydrol. 212–213, 198–212.

Bausch, W.C., Neale, C.M.U., 1989. Spectral inputs improve corn crop coefficients and irrigation scheduling. Trans. ASAE 32, 1901–1908.

Berk, A., Bernstein, L.S., Anderson, G.P., Acharya, P.K., Robertson, D.C., Chetwynd, J.H., Adler-Golden, S.M., 1998. MODTRAN cloud and multiple scattering upgrades with application to AVIRIS. Remote Sens. Environ. 65, 367–375.

Brotzge, J.A., Crawford, K.C., 2003. Examination of the surface energy budget: a comparison of eddy correlation and Bowen ratio measurement systems. J. Hydrometeorol. 4, 160–178.

Brutsaert, W., Sugita, M., 1992. Application of self preservation diurnal evolution of the surface energy budget to determine daily evaporation. J. Geophys. Res. 97, 18377–18382.

Chavez, J.L., Neale, C.M.U., Hipps, L.E., Prueger, J.H., Kustas, W.P., 2005. Comparing aircraft-based remotely sensed energy balance fluxes with eddy covariance tower data using heat flux source area functions. J. Hydromteorol. 6, 923–940.

Chehbouni, A., Lo Seen, D., Njoku, E.G., Monteney, B.M., 1996. Examination of difference between radiometric and aerodynamic surface temperature over sparsely vegetated surfaces. Remote Sens. Environ. 58, 177–186.

Choudhury, B.J., Ahmed, N.U., Idso, S.B., Reginato, R.J., Daughtry, C.S.T., 1994. Relations between evaporation coefficients and vegetation indices studied by model simulations. Remote Sens. Environ. 50, 1–17.

Colaizzi, P.D., Evett, S.R., Howell, T.A., Tolk, J.A., 2006. Comparison of five models to scale daily evapotranspiration from one-time-of-day measurements. Trans. ASAE 49 (5), 1409–1417.

Crago, R.D., 1996. Conservation and variability of the evaporative fraction during the daytime. J. Hydrol. 180, 173–194.

Crago, R.D., Brutsaert, W., 1996. A daytime evaporation and the self-preserve of the evaporative fraction and the Bowen ratio. J. Hydrol. 178, 241–255.

Doorembos, J., Pruitt, W.O., 1977. Crop water requirements. FAO Irrigation and Drainage Paper No. 24, Rome.

Gillies, R.T., Carlson, T.N., Cui, J., Kustas, W.P., Humes, K.S., 1997. A verification of the "triangle" method for obtaining surface soil water content and energy fluxes from remote measurements of the Normalized Difference Vegetation Index (NDVI) and surface radiant temperatures. Int. J. Remote Sens. 18 (15), 3145–3166, doi:10.1080/014311697217026.

Glenn, E., Huete, A., Nagler, P., Nelson, S., 2008. Relationship between remotely-sensed vegetation indices, canopy attributes and plant physiological processes: what vegetation indices can and cannot tell us about the landscape. Sensors 8 (4), 2136–2160.

Gonzalez-Dugo, M.P., Mateos, L., 2008. Spectral vegetation indices for benchmarking water productivity of irrigated cotton and sugarbeet crops. Agric. Water Manage. 95, 48–58.

Gonzalez-Dugo, M.P., Neale, C.M.U., Mateos, L., Kustas, W.P., Li, F., 2006. Comparison of remote sensing-based energy balance methods for estimating crop evapotranspiration. In: Owe, M., D'Urso, G., Neale, C.M.U., Gouweleeuw, B.T. (Eds.), Rem. Sens. for Agric. Ecosyst. Hidrol. Proc. SPIE, vol. 6359. p. 63590Z.

Gurney, R.J., Hsu, A.Y., 1990. Relating evaporative fraction to remotely sensed data at FIFE site. In: Symposium on FIFE: Fist ISLSCP Field Experiment, February 7–9. American Meteorological Society, Boston, pp. 112–116.

Hain, C.R., Mecikalski, J.R., Anderson, M.C., in press. Retrieval of an available water-based soil moisture proxy from thermal infrared remote sensing. Part I: Methodology and validation. J. Hydrometeorol.

Huete, A.R., 1988. A soil adjusted vegetation index (SAVI). Remote Sens. Environ. 25, 295–309.

Jackson, R.D., Moran, M.S., Gay, L.W., Raymond, L.H., 1987. Evaluating evaporation from field crops using airborne radiometry and ground based meteorological data. Irrig. Sci. 8, 81–90.

Kalma, J.D., MacVicar, T.R., McCabe, M.F., 2008. Estimating land surface evaporation: a review of methods using remotely sensed surface temperature data. Surv. Geophys., doi:10.1007/s10712-008-9037-z.

Kustas, W.P., 1990. Estimates of evapotranspiration with a one- and two-layer model of heat transfer over partial cover. J. Appl. Met. 29, 704–715.

Kustas, W.P., Choudhury, B.J., Moran, M.S., Reginato, R.D., Jackson, R.D., Gay, L.W., Weaver, H.L., 1989. Determination of sensible heat flux over sparse canopy using thermal infrared data. Agric. Forest Meteorol. 44, 197–216.

Kustas, W.P., Hatfield, J., Prueger, J.H., 2005. The soil moisture atmosphere coupling experiment (SMACEX): background, hydrometerological conditions and preliminary findings. J. Hydrometeorol. 6, 791–804.

Kustas, W.P., Norman, J.M., 1996. Use of remote sensing for evapotranspiration monitoring over land surfaces. Hydrol. Sci. 41, 495–516.

Kustas, W.P., Norman, J.M., 1997. A two-source approach for estimating turbulent fluxes using multiple angle thermal infrared observations. Water Resour. Res. 33, 1495–1508.

Kustas, W.P., Norman, J.M., 1999. Evaluation of soil and vegetation heat flux predictions using a simple two-source model with radiometric temperatures for partial canopy cover. Agric. Forest Meteorol. 94, 13–29.

Kustas, W.P., Norman, J.M., Schmugge, T.J., Anderson, M.C., 2004. Mapping surface energy fluxes with radiometric temperature (Chapter 7). In: Quattrochi, D., Luvall, J. (Eds.), Thermal Remote Sensing in Land Surface Processes. CRC Press, Boca Raton, FL, pp. 205–253.

Lhomme, J.-P., Monteny, B., Amadou, M., 1994. Estimating sensible heat flux from radiometric temperature over sparse millet. Agric. Forest Meteorol. 68, 77–91.

Li, F., Jackson, T.J., Kustas, W.P., Schmugge, T.J., French, A.N., Cosh, M.H., Bindlish, R., 2004. Deriving land surface temperature from Landsat 5 and 7 during SMEX02/SMACEX. Remote Sens. Environ. 92, 521–534.

Li, F., Kustas, W.P., Prueger, J.H., Neale, C.M.U., Jackson, J.T., 2005. Utility of remote sensing based two-source energy balance model under low and high vegetation cover conditions. J. Hydrometerol. 6, 878–891.

Mahrt, L., Vickers, D., 2004. Bulk formulation of the surface heat flux. Boundary Layer Meteorol. 110, 357–379.
Miller, D., 2006. SMEX02 Land Surface Information: Soils Database. National Snow and Ice Data Center. Digital Media, Boulder, Colorado, USA.
Monteith, J.L., Unsworth, M.H., 1990. Principles of Environmental Physics, 2nd ed. Edward Arnold, London.
Moran, M.S., Clarke, T.R., Inoue, Y., Vidal, A., 1994. Estimating crop water deficit using the relation between surface-air temperature and spectral vegetation index. Remote Sens. Environ. 49, 246–263, doi:10.1016/0034-4257(94)90020-5.
Moran, M.S., Jackson, R.D., Slater, P.N., Teillet, P.M., 1991. Comparison of atmospheric correction procedures for visible and near-IR satellite sensor output. In: Proceedings of the 5th International Colloquium. Physical Measurements and Signatures in Remote Sensing, Courchevel, pp. 7–12.
Neale, C.M.U., Bausch, W.C., Heermann, D.F., 1989. Development of reflectance based crop coefficients for corn. Trans. ASAE 32 (6), 1891–1899.
Norman, J.M., Kustas, W.P., Prueger, J.H., Diak, G.R., 2000. Surface flux estimation using radiometric temperature: a dual-temperature-difference method to minimize measurement errors. Water Resour. Res. 36 (8), 2263–2274.
Norman, J.M., Anderson, M.C., Kustas, W.P., 2006. Are single-source, remote-sensing surface-flux models too simple? In: D'Urso, G., Osann Fochum, M.A., Moreno, J. (Eds.), Proceeding of the International Conference on Earth Observation for Vegetation Monitoring and Water Management, AIP, vol. 852. pp. 170–177.
Norman, J.M., Kustas, W.P., Humes, K.S., 1995. A two-source approach for estimating soil and vegetation energy fluxes in observations of directional radiometric surface temperature. Agric. Forest Meteorol. 77, 263–293.
Priestley, C.H.B., Taylor, R.J., 1972. On the assessment of surface heat flux and evaporation using large scale parameters. Mon. Weather Rev. 100, 81–92, doi:10.1175/1520-0493(1972)100<0081:OTAOSH>2.3.CO;2.
Prueger, J.H., Hatfield, J.L., Kustas, W.P., Hipps, L.E., MacPherson, J.I., Neale, C.M.U., Eichinger, W.E., Cooper, D.I., Parkin, T.B., 2005. Tower and aircraft eddy covariance measurements of water vapor, energy, and carbon dioxide fluxes during SMACEX. J. Hydrometerol. 6, 954–960.
Romero, M.G., 2004. Daily evapotranspiration estimation by means of evaporative fraction and reference evapotranspiration fraction. Ph.D. Dissertation, Utah State Univ. Logan, Utah.
Shuttelworth, W., Wallace, J., 1985. Evaporation from sparse crops: an energy combination theory. Q. J. R. Meteorol. Soc. 111, 1143–1162.
Soil Survey Staff, Natural Resources Conservation Service, United States Department of Agriculture. Official Soil Series Descriptions [Online WWW]. Available URL: http://soils.usda.gov/technical/classification/osd/index.html (Accessed on October 2008).
Timmermans, W.J., Kustas, W.P., Anderson, M.C., French, A.N., 2007. An intercomparison of the surface energy balance algorithm for land (SEBAL) and the two-source energy balance (TSEB) modeling schemes. Remote Sens. Environ. 108, 284–369.
Twine, T.E., Kustas, W.P., Norman, J.M., Cook, D.R., Houser, P.R., Meyer, T.P., Prueger, J.H., Starks, P.J., Wesley, M.L., 2000. Correcting eddy-covariance flux underestimates over grassland. Agric. Forest Meteorol. 103, 279–300.
Wright, J.L., 1982. New evapotranspiration crop coefficients. J. Irrig. Drain. Div. 108, 57–74.